http://www.raa-journal.org   *http://iopscience.iop.org/raa*

*R*esearch in
*A*stronomy and
*A*strophysics

MHD simulations of inward shocks in Cassiopeia A

Chu-Yuan Yang[1,2,3], Bi-Wen Bao[4] and Si-Ming Liu[5]

[1] Yunnan Observatories, Chinese Academy of Sciences, Kunming 650216, China; *chyy@ynao.ac.cn*
[2] Key Laboratory for the Structure and Evolution of Celestial Objects, Chinese Academy of Sciences, Kunming 650216, China
[3] Center for Astronomical Mega-Science, Chinese Academy of Sciences, Beijing 100101, China
[4] Department of Astronomy, Key Laboratory of Astroparticle Physics of Yunnan Province, Yunnan University, Kunming 650091, China; *baobiwen@ynu.edu.cn*
[5] Key Laboratory of Dark Matter and Space Astronomy, Purple Mountain Observatory, Chinese Academy of Sciences, Nanjing 210033, China; *liusm@pmo.ac.cn*

Abstract Cassiopeia A, the brightest radio supernova remnant (SNR) in the sky, has several unique characteristics in comparison to its peers. Besides its radio brightness and prominent soft-concave radio spectrum, its γ-ray spectrum appears to have a low-energy cutoff near 2 GeV, and it is the only SNR with prominent hard X-ray emission. While the unusual radio properties may be attributed to strong emission from reverse shocks, the hard X-ray emission has been associated with high-speed inward shocks induced by high density gases. Then, the low-energy γ-ray spectral cutoff could be attributed to slow penetration of lower energy particles accelerated near the inward shocks into high-density emission zone. In this paper, we carry out magneto-hydrodynamic (MHD) simulations of shocks in Cassiopeia A and demonstrate that its inward shock structure can indeed be reproduced via shock interactions with clumps of gases with a density of $\sim 20\,\mathrm{cm}^{-3}$.

Key words: acceleration of particles — supernovae: individual (Cassiopeia A) — ISM: supernova remnants — X-rays: ISM

1 INTRODUCTION

Cassiopeia A (hereafter Cas A), a young Galactic supernova remnant (SNR) with an estimated age of ~ 340 years, has long been considered as an ideal candidate for testing the SNR origin of galactic cosmic rays. With the help of high resolution multi-wavelength observations, basic properties of Cas A (such as distance, age, explosion type, and environment) have been well-constrained (Reed et al. 1995; DeLaney & Rudnick 2003; Hwang & Laming 2003; Fesen et al. 2006; Krause et al. 2008). Although Cas A is very bright in radio implying very efficient electron acceleration and strong magnetic fields, its γ-ray flux is relatively low, especially in light of the high density of shocked X-ray emitting plasmas, which give rise to a relatively low ion acceleration efficiency (Vink et al. 2010). Moreover, nonthermal emission from Cas A has several distinct properties, such as a soft-concave radio spectrum, prominent hard X-ray emission, and γ-ray spectral cutoffs at both low- and high-energies (Zhang & Liu 2019). Besides, emission associated with forward and reverse shocks, inward shocks induced by shock collision with high density gases have been proposed for the hard X-ray emission (Sato et al. 2018). Forward and reverse shocks of SNRs arise from interaction between ejecta of the supernovae and surrounding medium. With regard to Cas A, the common consensus is that the remnant evolves in a complex circumstellar medium produced by its progenitor system (Chevalier & Oishi 2003; Vink 2004; Hwang & Laming 2009) along with an anisotropic ejecta profile (DeLaney et al. 2010; Milisavljevic & Fesen 2013, 2015). Recent observations imply an association between the shock front of Cas A and molecular clouds (Keohane et al. 1996; Fesen et al. 2011; Kilpatrick et al. 2014). However, new results of CO observations towards Cas A seem to cast some doubts on this issue and the authors argue that there is no clear physical evidence to support that Cas A is interacting with molecular clouds (Zhou et al. 2018).

The latest evidence for shock collision with high density gases comes from analyzing bright nonthermal X-ray emission features inside Cas A based on *Chandra* and *NuSTAR* observations (Sato et al. 2018). The most striking result is the identification of several bright inward-moving X-ray filaments. Such inward-moving filaments, as the authors claimed, are triggered by fast inward-moving shocks. By measuring the proper-motion of these inward shocks, they inferred that the velocity was about $\sim 2100 - 3800 \, \mathrm{km \, s^{-1}}$ for a distance of 3.4 kpc. Considering Cas A's young dynamical age, it is implausible to expect an inward-moving reverse shock in the observer frame. The authors proposed instead that these inward shocks were caused by interaction between the forward shock and dense gases in the circumstellar medium with an estimated density jump of about $5 - 8$, reminiscent of the well-studied SNR 1987A (Pun et al. 2002).

Motivated by these results, we perform two-dimensional (2D) magnetohydrodynamic (MHD) simulations of SNR shocks and demonstrate that inward shock structure in Cas A can indeed be reproduced via shock interactions with dense gases. The structure of this paper is as follows. A detailed description of our model and initial setup of simulations are in Section 2. The simulation results are presented in Section 3, while some discussion and conclusions are given in Section 4.

2 MODEL DESCRIPTION

Our purpose here is to reproduce forward, reverse, and inward shock structure of Cas A by 2D-MHD simulations assuming cylindrical-symmetry except for turbulent fluctuations. The simulations are carried out in the domain with $x \in [0, 5] \, \mathrm{pc}$ and $y \in [-5, 5] \, \mathrm{pc}$ on 1024×2048 uniform grids.

The mean background magnetic field $B_0 = 3 \, \mu\mathrm{G}$ is along the y-axis, the ambient gas number density $n_\mathrm{H} = 1.0 \, \mathrm{cm^{-3}}$, and the background temperature $T_0 = 10^4 \, \mathrm{K}$. The shock wave is driven via injecting thermal energy and mass in a small circular region with a radius of 0.5 pc centered at the origin of the coordinates. We assume an SNR age of 20 years for this initial setup. The detailed setting of the initial profile of the ejecta can be found in Jun & Norman (1996); Fang et al. (2018) with the ejecta energy $E_\mathrm{ej} = 2 \times 10^{51}$ erg, ejecta mass $M_\mathrm{ej} = 2 \, M_\odot$. The ejecta magnetic field is turbulent with $\langle \delta B^2 \rangle = (300 \, \mu\mathrm{G})^2$ and a coherent length of 0.1 pc (Wang et al. 2018). The Rayleigh-Taylor instability in the shock region is seeded by inserting a random component of the ejecta density with a maximum magnitude of $\sim 10\%$.

Forward and reverse shocks naturally emerge with the initial setup given above. To produce inward shocks, we consider "reflection shocks" produced by collisions of the forward shock with high density clumpy gases in the ambient medium. Such clumps may be the outcomes of progenitor system which have suffered from a Wolf-Rayet phase (van Veelen et al. 2009). According to observations of X-ray filaments associated with inward shocks, these dense gases should have a relatively high density and a small filling factor. We add to the above setup four uniform circular dense gases within $(x - x_i)^2 + (y - y_i)^2 \leq (0.2\mathrm{pc})^2$, where (x_i, y_i) is the center coordinates of these gases with $i = 1, 2, 3, 4$, and $(x_1, x_2, x_3, x_4) \rightarrow (0, 2.1 \sin(\pi/8), 2.1 \sin(\pi/4), 2.1 \sin(3\pi/8))$ pc, and $y_i = \sqrt{2.1^2 - x_i^2}$ so that the forward shock started interacting with these dense gases about ~ 100 yr ago as suggested by observations (see Sato et al. 2018). The dynamical evolution of the SNR are then calculated by using the PLUTO code (Mignone et al. 2007, 2012). In our simulation, the MHD equations are solved with the cell-centered finite-volume scheme with high-order Godunov methods. The magnetic field is evolved with the constrained transport technique to preserve the divergence-free condition, and the fluxes are calculated using the Harten-Lax-Van Leer Riemann solver. Moreover, we use the outflow condition as our boundary condition in each dimension and adopt the harmonic mean limiter of Van Leer.

3 SIMULATION AND RESULTS

Based on X-ray observations, Sato et al. (2018) estimated that the inward shocks were produced by forward shocks plunging into dense plasmas with a $\gtrsim 5 - 8$ times higher density enhancement relative to the background. Here, we run simulations with a dense gas density $n_\mathrm{g} = 8, 24$, and $72 \, \mathrm{cm^{-3}}$, respectively. Figure 1 shows the corresponding results. As expected, the magnetic field is strongest near the contact discontinuity between the ejecta and the ambient medium due to amplification via the Rayleigh-Taylor instability (Guo et al. 2012). Since dense gases are located in the upper half of the simulation domain ($y > 0$), the lower half shows the forward and reverse shocks unaffected by the four clumps of dense gas.

The left panel of Figure 2 shows the evolution of the average speed of the forward and reverse shocks obtained from the lower half of the simulation domain ($y < 0$). The right and middle panels show the corresponding speed distribution. As expected, both forward and reverse shocks are moving outward at the current age of 340 years with an average speed of ~ 5000 and $\sim 3000 \mathrm{km \, s^{-1}}$ in the observer frame, respectively.
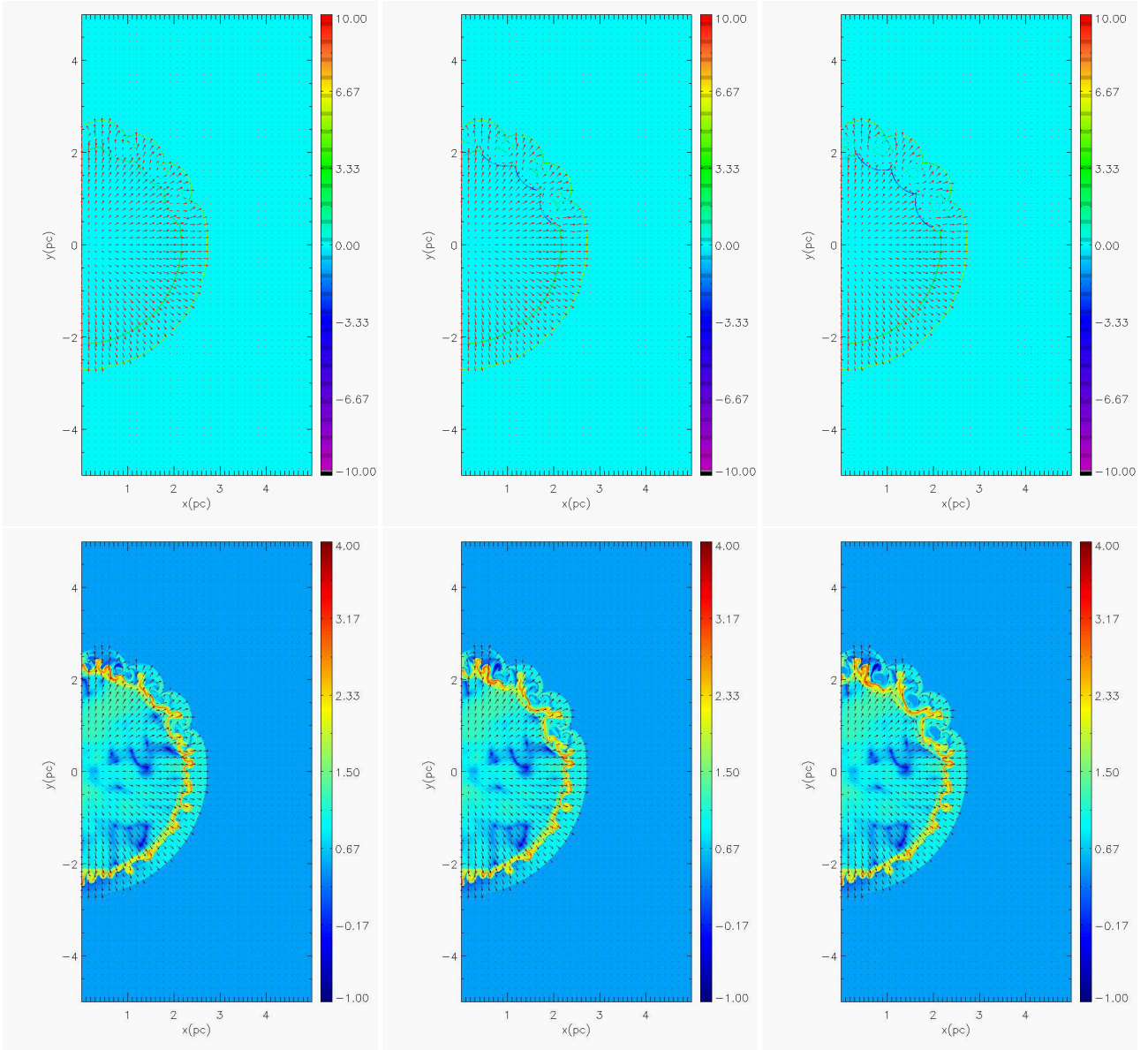
Fig. 1 The shock structure (*top*) and magnetic field (*bottom*) of simulations at an SNR age of 340 yr for a dense gas density of $n_g = 8$ (*left*), 24 (*middle*), and 72 (*right*) cm^{-3}, respectively. The *color bars* in the top and the bottom panel show the shock speed in units of $1000 \, km \, s^{-1}$ and the logarithmic of the magnetic field in units of μG, respectively. Negative speed represents propagation inward. The *arrows* show the two-dimensional velocity field with the arrow length proportional to the velocity amplitude.
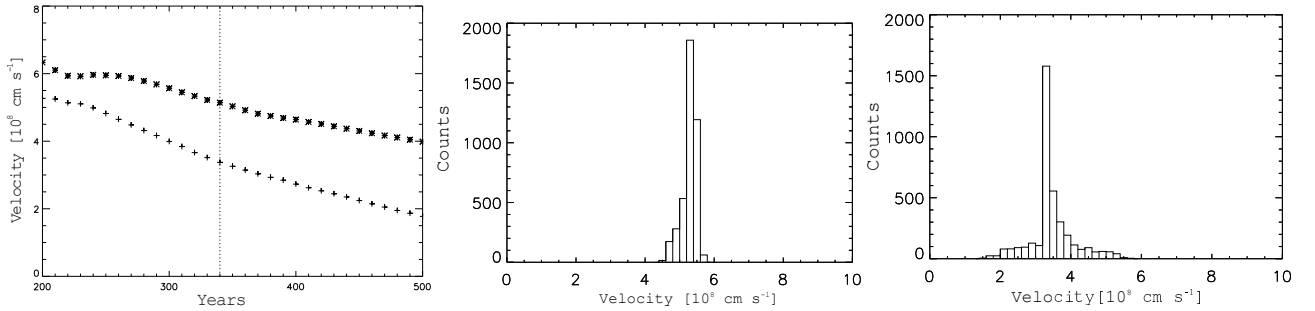
Fig. 2 *Left*: Evolution of the average shock speed in a uniform circumstellar medium. Forward shock is indicated by the *asterisks* and reverse shock by the *plus signs*. The *vertical dotted line* indicates the current age of the remnant. *Middle* and *right* panels show the speed distribution of the forward and reverse shocks at 340 years, respectively (the shock speed is in units of $1000 \, km \, s^{-1}$) .
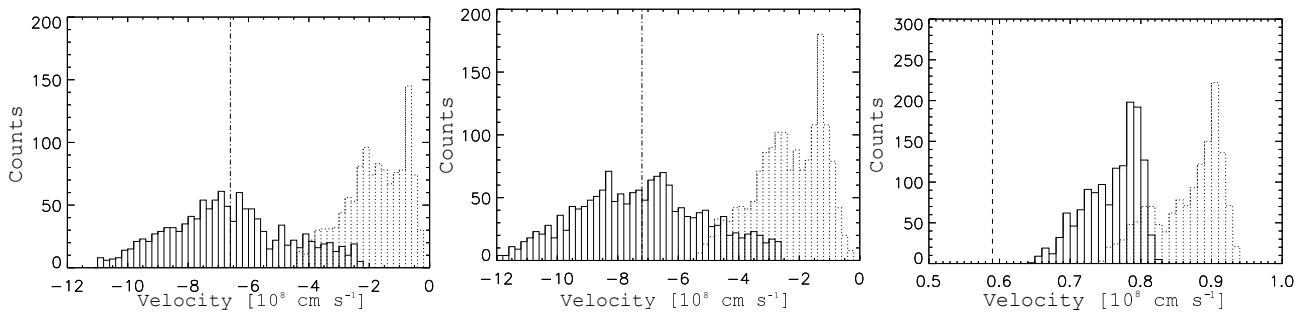
Fig. 3 Speed distribution of inward shock at the age of 340 yr for $n_{\rm g} = 24\,{\rm cm}^{-3}$ (*left panel*) and $n_{\rm g} = 72\,{\rm cm}^{-3}$ (*middle panel*), respectively (the shock speed is in units of $1000\,{\rm km\,s}^{-1}$). The *solid* and *dotted lines* represent the shock speed in the ejecta frame and the shock radial velocity in the observer frame, respectively. The *dash-dotted line* shows the average shock speed in the ejecta frame. *Right panel*: The distribution of radial thickness between the forward and the inward shocks at the age of 340 yr for $n_{\rm g} = 24\,{\rm cm}^{-3}$ (*solid line*) and $n_{\rm g} = 72\,{\rm cm}^{-3}$ (*dotted line*), respectively (the thickness is in units of pc). The *dashed line* indicates the averaged radial thickness between the forward and reverse shocks derived from the lower part of the simulation domain ($y < 0$).

The presence of dense gases in the upper simulation domain modifies the shock structure significantly. But for $n_{\rm g} = 8\,{\rm cm}^{-3}$ (left panel of Fig. 1), the "reflective shocks" induced by collision of forward shocks with these dense gases are still moving outward and therefore cannot account for the inward-moving X-ray filaments observed in Cas A. For $n_{\rm g} = 24$ (middle) and $72\,{\rm cm}^{-3}$ (right panel of Fig. 1), however, a significant fraction of the "reflective shocks" are moving inward. The left and middle panels of Figure 3 show the radial velocity (dashed) and speed (solid) distributions of the reflective shocks in the observer and ejecta frames, respectively. The speed of the inward shocks increase with the increase of $n_{\rm g}$. The right panel of Figure 3 shows the distribution of the radial thickness between the forward and inward shocks. This thickness distributes in $0.65 - 0.82$ and $0.75 - 0.94$ pc for $n_{\rm g} = 24$ and $72\,{\rm cm}^{-3}$, respectively, which is larger than the mean thickness of ~ 0.6 pc between the forward and reverse shocks in the normal regions ($y < 0$), and this thickness also increases with the increase of $n_{\rm g}$. Since particle acceleration is most efficient near the shock front and the observed nonthermal X-ray emission is likely dominated by very high-energy electrons via the synchrotron process, it is reasonable to associate the observed X-ray filaments with the shock fronts. Then we find that the case with $n_{\rm g} = 24\,{\rm cm}^{-3}$ can reproduce the observed thickness of ~ 0.7 pc and the observed inward shock speed of $\sim 5100 - 8700\,{\rm km\,s}^{-1}$ (Sato et al. 2018).

4 DISCUSSION AND CONCLUSIONS

Via MHD simulations of supernova ejecta evolution in a clumpy circumstellar medium, we reproduce complex shock structures observed in Cas A, especially inward shocks associated with prominent hard X-ray emission and X-ray filaments (Sato et al. 2018). Our simulations also lead to a constraint of $\sim 20\,{\rm cm}^{-3}$ on the density of the

dense gases responsible for the inward shock. A gas density of $\sim 10\,{\rm cm}^{-3}$ is not high enough to induce inward shocks at the current stage of the SNR evolution. A much higher density will lead to higher inward shock speed and larger separation between the inward and forward shocks. Given the limitation of 2D simulations, as well as the anisotropy of the ejecta, our constraint on the density may not be accurate. Our study shows that observed inward shock speed and location may lead to a measurement of the density of dense gases. Therefore, 3D simulations with synthetic X-ray emitting structures are warranted for better comparison with observations (see Orlando et al. 2016 for a 3D attempt). However, it should be noted that recent results of CO observations towards Cas A disfavor shock-cloud interaction scenario and we suggest that this issue should remain open for further discussion (Zhou et al. 2018).

In our simulation, the spatial resolution is about $0.005{\rm pc} \times 0.005{\rm pc}$, which can resolve the width of ~ 0.1 pc for strongly magnetized regions near the contact discontinuity between the ejecta and circumstellar medium (see the bottom panels of Fig. 1). Both the Rayleigh-Taylor instability and the turbulent magnetic field in the ejecta contribute to the magnetic field amplification (see Guo et al. 2012; Yang & Liu 2013; Bao et al. 2018). The amplification is enhanced near the dense gases with the magnetic field reaching to a few milli-Gauss.

Observations of Cas A's nonthermal emission reveal several unique features (Zhang & Liu 2019). While the prominent hard X-ray emission may be attributed to high-speed inward shocks, the origin of the low-energy cutoff of the GeV emission is very puzzling. Zhang & Liu (2019) proposed a two zone model for nonthermal emission from Cas A, where most of the GeV emission originates from penetration of high-energy particles accelerated at the inward shocks into high density gases. According to our sim-

ulations, the dense gases are separated from the inward shocks by a layer of strongly magnetized plasma, which can slow down diffusion of relatively low-energy relativistic particles in the dense emission zone. Coupling of MHD simulations with particle acceleration and transport models will be able to advance our understanding of cosmic rays acceleration and the nonthermal emission in Cas A significantly.

References

Bao, B., Yang, C., & Zhang, L. 2018, ApJ, 866, 37

Chevalier, R. A., & Oishi, J. 2003, ApJ, 593, L23

DeLaney, T., & Rudnick, L. 2003, ApJ, 589, 818

DeLaney, T., Rudnick, L., Stage, M. D., et al. 2010, ApJ, 725, 2038

Fang, J., Yu, H., & Zhang, L. 2018, MNRAS, 474, 2544

Fesen, R. A., Zastrow, J. A., Hammell, M. C., Shull, J. M., & Silvia, D. W. 2011, ApJ, 736, 109

Fesen, R. A., Hammell, M. C., Morse, J., et al. 2006, ApJ, 645, 283

Guo, F., Li, S., Li, H., et al. 2012, ApJ, 747, 98

Hwang, U., & Laming, J. M. 2003, ApJ, 597, 362

Hwang, U., & Laming, J. M. 2009, ApJ, 703, 883

Jun, B.-I., & Norman, M. L. 1996, ApJ, 465, 800

Keohane, J. W., Rudnick, L., & Anderson, M. C. 1996, ApJ, 466, 309

Kilpatrick, C. D., Bieging, J. H., & Rieke, G. H. 2014, ApJ, 796, 144

Krause, O., Birkmann, S. M., Usuda, T., et al. 2008, Science, 320, 1195

Mignone, A., Bodo, G., Massaglia, S., et al. 2007, ApJS, 170, 228

Mignone, A., Zanni, C., Tzeferacos, P., et al. 2012, ApJS, 198, 7

Milisavljevic, D., & Fesen, R. A. 2013, ApJ, 772, 134

Milisavljevic, D., & Fesen, R. A. 2015, Science, 347, 526

Orlando, S., Miceli, M., Pumo, M. L., & Bocchino, F. 2016, ApJ, 822, 22

Pun, C. S. J., Michael, E., Zhekov, S. A., et al. 2002, ApJ, 572, 906

Reed, J. E., Hester, J. J., Fabian, A. C., & Winkler, P. F. 1995, ApJ, 440, 706

Sato, T., Katsuda, S., Morii, M., et al. 2018, ApJ, 853, 46

van Veelen, B., Langer, N., Vink, J., García-Segura, G., & van Marle, A. J. 2009, A&A, 503, 495

Vink, J. 2004, New Astron. Rev., 48, 61

Vink, J., Yamazaki, R., Helder, E. A. 2010, ApJ, 722, 1727

Wang, Y., Bao, B., Yang, C., & Zhang, L. 2018, MNRAS, 478, 2948

Yang, C., & Liu, S. 2013, ApJ, 773, 138

Zhang, X., & Liu, S. 2019, ApJ, 874, 98

Zhou, P., Li, J.-T., Zhang, Z.-Y., et al. 2018, ApJ, 865, 6